Eindhoven University of Technology
Eindhoven, The Netherlands
June 19, 2025

Bio-based 3D printing and testing of a digitally designed structural element

Franka Evalien PELS RIJCKEN* ir. Arjan HABRAKEN[a], dr. ir. Faas MOONEN[a]

*Department of the Built Environment, Structural Engineering and Design
Eindhoven University of Technology, The Netherlands
f.e.pels.rijcken@student.tue.nl, a.p.h.w.habraken@tue.nl, s.p.g.moonen@tue.nl

Abstract

In order to design and fabricate a parametric structural element made from a bio-based material using additive manufacturing, a newly developed 3D printable material was investigated. The material was inspired by the work of Bierach and Coelho (2022), who developed two promising mixtures consisting of cellulose, lignin and a binder: methylcellulose (MC) or wood glue (WG). These two mixtures were improved by adjusting the compositions and also a third binder (bio-glue (BG)) was investigated. The best performing mixtures combined cellulose, lignin and Valida L,3 % with WG or BG. Mechanical tests were performed to determine the mechanical properties of these mixtures. Despite the slightly higher strength of WG, the BG mixture was preferred because of its fully bio-based composition. The mechanical properties of the BG mixture were improved by the addition of flax fibres. A truss-like beam was digitally designed, optimised and printed using the BG with flax mixture. It was subjected to a bending test and results indicate that the structural strength and behaviour of this newly developed bio-based material is promising. The new material shows great potential for the building industry, as its mechanical properties are comparable to those of other low-strength materials already in use. At the moment, the material's strength and stiffness are not structurally safe. And therefore, this needs further research to become suitable for structural applications.

Keywords: Bio-based material, wood printing, cellulose, lignin, flax fibres, additive manufacturing, liquid deposition modeling (LDM), mechanical testing, parametric design, structural optimization

1 Introduction

Global warming is a worldwide phenomenon that is affecting us all, threatening life as we know it, and is caused primarily by the increasing emissions of greenhouse gases (GHG) due to human activities. The consequences of rising global temperatures include, amongst others, rising sea levels, declining biodiversity, desertification and more frequent and more destructive natural disasters [1], [2]. The building industry is a major contributor to this climate crisis, accounting for 35% of the total global CO_2 emissions [3]. In response to this global crisis, the Netherlands has signed the United Nations Paris Climate Accord, an international treaty that aims to limit global warming by reducing GHG emissions by 50% by 2030 [4]. In addition, the Rijksoverheid (Dutch government) has set a target of achieving a circular and bio-based economy by 2050 [5]. The Dutch building industry consumes 40% of the total energy and, 50% of all the raw materials used in the Netherlands, and is also responsible for 40% of the total waste production. Consequently, the building sector is responsible for 35% of the total carbon dioxide (CO_2) emissions in the Netherlands [5]. In response, various plans have been initiated to reduce the CO_2 pollution of this sector. For example, one of the goals of the Rijksoverheid is to reduce the use of primary resources by 50% [5]. Possible methods to reach this are to reduce the use of raw materials, to maximise the use of renewable resources or to optimise the material usage during the whole lifecycle of a building. This was explored in this study by designing a structural element (beam) using a new bio-based material, and additive manufacturing (AM) was utilised to produce this beam. AM has been developed as an environmentally friendly and sustainable technology capable of reducing material usage and energy consumption. It provides the freedom to design and produce unique elements due to its high level of precision and the fact that formwork is not required. Furthermore, AM has additional benefits, such as reduced waste production, decreased physical labour and increased construction speed [6]. To

exploit the benefits of this innovative technology, the beam is digitally designed and optimised to use as little material as possible in order to reduce the potential CO_2 emissions [7].
Bio-based materials, all or significant part, originate from renewable resources. The most CO_2-neutral bio-based materials are made from locally sourced materials, which can be raw resources from nature or materials that are often regarded as waste [8], [9]. The utilisation of bio-based materials in the building sector has the potential to significantly decrease (ranging from 10-50%) of the GHG emissions [9], [10]. A number of bio-based materials, such as timber, are successfully used in the construction industry. However, new bio-based materials still face many challenges, including industry and societal perceptions of their durability and reliability as a construction material [11]. Further research and experimental testing of bio-based materials is required to determine the materials and mechanical properties, and to ensure their structural safety.
This study is part of the Innovative Structural Engineering and Design (ISD) research field at the Eindhoven University of Technology (TU/e). The objective of the study is to design and fabricate a parametric structural element made from a bio-based material using additive manufacturing. In light of the recognised impact of CO_2 emissions on the planet [1], it was decided to prioritise the use of bio-based materials, rather than focusing purely on its mechanical properties.

2 State of the art bio-based 3D printing

Additive manufacturing (AM), or 3D printing, is widely utilised by a variety of industries, such as medicine, aerospace, automotive, food and military industries. A wide variety of materials can be used, including ceramics, plastics, concrete and bio-composite materials [12].
Several AM methods are available (Figure 1) and each method has its own (dis)advantages and they should therefore be carefully selected, based on the material composition and properties as well as the desired product [13]. Table 1 lists some 3D printed bio-based materials. Commonly, bio-based materials are printed using material extrusions like fused deposition modeling (FDM) or liquid deposition modeling (LDM).

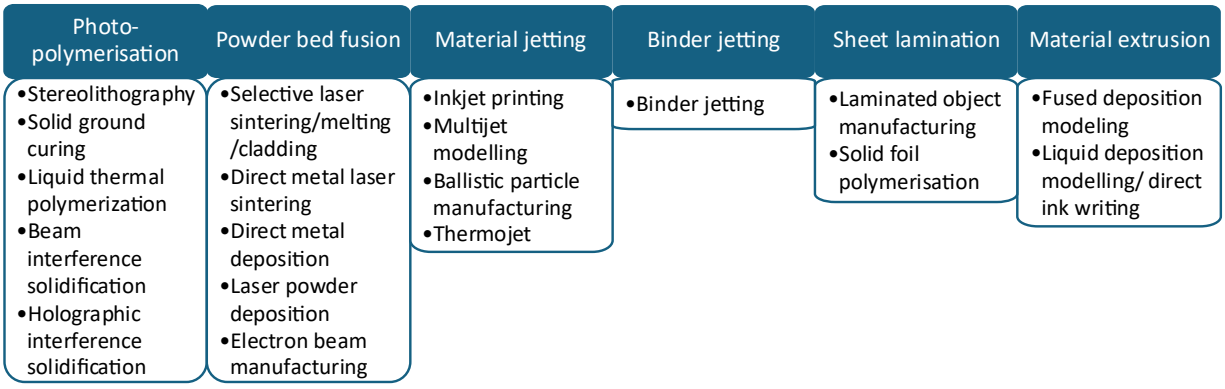

Figure 1. Categories of additive manufacturing processes [13], [14].

Based on the available equipment and knowledge regarding extrusion-based 3D printing at the TU/e, the LDM method was selected in this project. LDM is considered to be one of the most versatile AM methods as it enables the utilisation of a wide range of materials, provided that the material can be engineered to have the appropriate rheological properties. The fresh material should be extrudable, self-standing and adhere to the previous layers. The exact rheological properties depend on the material utilised and the desired printed product. The material is extruded through a nozzle and additional heat is not required. The pressure, flow rates, and diameter of the nozzle can be easily controlled. After extrusion, the material solidifies, either naturally or assisted by external processes such as evaporation or heat treatment [15], [16], [17]. During the solidification process the material should build up its mechanical strength [18]. Furthermore, sufficient bond strength should be developed so that the whole printed element ideally breaks before the layers start to separate [19].

Table 1. Projects dealing with additive manufacturing using bio-based materials.

AM method	(Main) Material	Project / product name	References
FDM	Polylactic acid (PLA)	-	BCN3D [20]
	PLA – wood composite	Conifera	Mamou-Mani Ltd [21]
	Algae based polymers	Wierwaar	Klarenbeek and Dros [22]
LDM	Soil	Gaia House	WASP [23], [24]
		TECLA	WASP and Mario Cucinella Architects [25], [26]
	Seed-impregnated soil	Living soil	
	Ceramic	-	San Fratello [27], van Herpt [28], Mamou-Mani [29]
	Sewage water treatment residuals	BuildMatterial	Omlab [30]
	Mycelium	-	Klarenbeek [31] , Blast Studio [32]
	Wood powder	-	Kariz et al.[33] , Rosenthal et al. [34]
	Cellulose and lignin	Wood-based printing	A. Coelho [35] and C. Bierach [36]
Binder jetting	Sand	-	Sandhelden [37]
		Sandwaves	Precht and Mamou-Mani Ltd [38], [39]

Due to the scale of this research, the level of expertise and the availability of materials, it was decided to focus on wood-based printing. Cellulose and lignin, the two primary components of wood, are one of the most abundant organic polymers on earth. Although these polymers are being utilised in many applications, for instance as additives, they have not often been combined [40]. As demonstrated by research conducted at TU Delft [35], [36], wood-based printing has great potential in a variety of applications, however, further studies and improvements are necessary for its use in structural elements. It was decided to use the wood glue (WG) and methylcellulose (MC) mixtures from TU Delft as reference mixtures, see Table 2 for their compositions. The WG mixture was included due to its better mechanical properties although it was not 100% bio-based.

Table 2. Mixtures compositions by A. Coelho and C. Bierach [35], [36].

Binder type	Content of component			
	Cellulose	Lignin	Water	Binder
Methylcellulose	2.9%	29.1%	63.1%	4.9%
Wood glue	2.4%	24.4%		73.2%

The mechanical properties of these mixtures could be improved by substituting or adding materials. Table 3 provides the possible materials. which are divided into three categories: raw materials, binders and additives. An additive is a substance that is added to a mixture to improve different parameters of its properties. They can boost existing properties, suppress unwanted properties or even introduce new properties [41].

Table 3. Possible materials divided into three categories.

Raw material	Binder	Additives
Cellulose	Methylcellulose	Bentonite
Lignin	Wood glue	Natural fibres
	Bio-based glue	

Bentonite, a non-toxic type of clay, is found across the globe, including in North America, Europe and Asia. It is an economic, environmentally friendly and high-performance rheological additive, which provides excellent rheological properties such as viscosity, shear-thinning behaviour and thixotropy [42], [43]. The benefits of bentonite as an additive in wood-based 3D printable mixtures has been demonstrated by Bierach and Coelho, who demonstrated that bentonite improved the adhesion, the stability and stiffness of the fresh mixture and cured products [35], [36].
Natural fibres are a popular eco-friendly reinforcement, due to their abundancy, renewability, sustainability and ease of processing [44]. Numerous studies have demonstrated that the addition of natural fibres into 3D concrete printing (3DCP) mixtures resulted in improved mechanical properties, especially the tensile and flexural strength [44], [45], [46], [47]. In addition, these fibres have demonstrated to reduce the crack width, lower the shrinkage, improve the mechanical properties and enhance the fresh and rheological characteristics [44]. Coelho demonstrated that adding 10 mm long

flax fibres to the wood-based mixture, resulted in improved strength of the cured product [35]. However, excess addition of fibres can form a challenge in the extrusion process, leading a diminished workability and a reduced mechanical strength [44], [45].

3 Material exploration

The first objective was to gain an understanding of the interactions between the cellulose and lignin with various binders, and the second to find the most optimal mixture compositions with the different binders. This was investigated in three distinct phases. At first, the mixtures from Coelho and Bierach were recreated and evaluated on their fresh and cured properties. Subsequently, the compositions and mixing processes were altered to accommodate the available materials and equipment. Finally, two reference mixtures were selected for print testing and for the further testing of the mechanical behaviour and strength and the exploration of the addition of additives.
It is noted that, in general, the period between mixing and printing slightly fluctuated. Whether this had an impact on the material was however not investigated in this initial study

3.1 Mixtures

Figure 2 schematically describes how the mixtures were investigated. After extrusion, the mixture was given a rating, which was based on manual assessment and visual observations. For the fresh state, assessments were made for the homogeneity, extrudability and adhesion. After the material had cured, assessments were made for the failure behaviour and the curing time. After this, it was determined whether the mixture could be improved. If necessary, the composition was modified, and the process was restarted. This process was repeated until an optimal mixture was finally found.

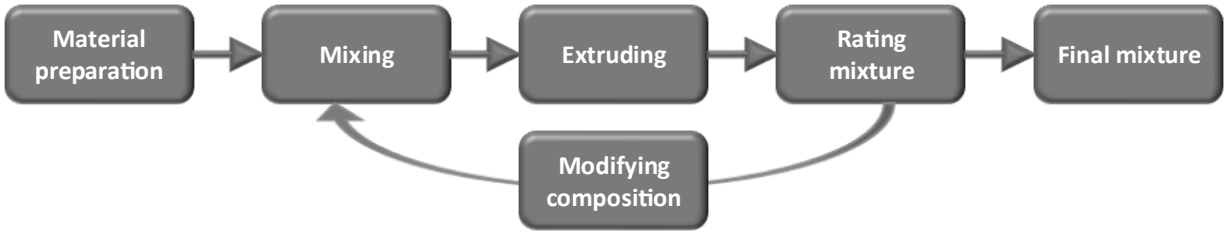

Figure 2. Mixture exploration process

3.1.1 Methylcellulose

Several attempts, although unsuccessful, were made to adjust and improve the MC mixtures. The mixtures remained too viscous and displayed poor extrudability, homogeneity and adhesion. Moreover, the cured elements simply fell apart. After several days the elements started to grow mould, which could not be prevented. Due to these poor results, the use of the MC mixtures was rejected.

3.1.2 Wood glue

The WG mixtures from Coelho and Bierach were successfully recreated, however, resulting in a mixture with a bio-based content of only 20% due to the high wood glue content. After several repeats and the addition of Valida L, 3% (fibrillated nanocellulose) [48] to the mixture, a promising mixture with a bio-based content of 57% was produced (Table 4). This mixture had excellent properties and great potential to be improved regarding its mechanical properties. And despite not being 100% bio-based, it was selected as the first reference mixture for further investigation.

3.1.3 Bio-glue

A third mixture composition was formulated, in which the wood glue was substituted with bio-glue (BG), resulting in a 100% bio-based mixture (Table 4). The fresh and cured properties of this mixture also yielded high ratings and was therefore selected as the second reference mixture.

Table 4. Wood glue and bio-glue mixtures compositions

Glue type	Content of component [gram]			
	Cellulose	Lignin	Valida L,3%	Glue
Wood glue	25	200	300	400
Bio-glue	30	300	300	450

3.2 Curing process

During material exploration, various curing conditions were investigated. This included different curing temperatures and different coverings. The climate room at the structures laboratory (SED-lab) at the TU/e was selected as the most optimal curing location due to its constant temperature of 20 °C and an average relative humidity (RH) of 60%. The most optimal covering was a thin plastic film. The initial curing process was roughly 21 days: around 7 days with a plastic film cover, around 7 days without a cover, and finally around 7 days with the beams turned upside down, in order to limit warping.

4 Robotic printing

The robot used in this study was the ABB IRB 1200- 5/0.9, a six-axis robot with six degrees of freedom (DOF), a loading capacity of five kilograms, and a radius of 0.9 metres [49]. This robot was available in the SED-lab and was equipped with a Makita caulk gun through a steel connector element (Figure 3). The Makita uses a piston (push bar) to extrude material by applying pressure to the contents of the cartridge. For the fabrication of the test beams, a rectangular nozzle was used, and for the structural beam, a round nozzle was used (Figure 4).

Figure 3. ABB IRB 1200- 5/0.9 with the Makita.

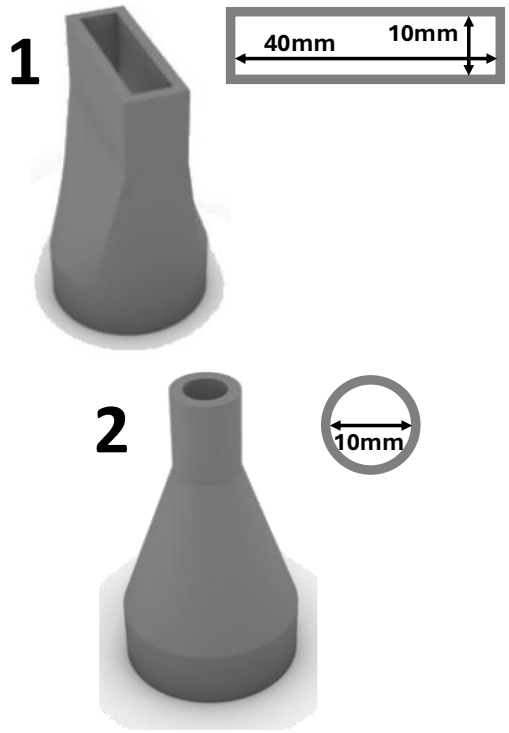

Figure 4. The rectangular nozzle (1) and the round nozzle (2).

5 Mechanical properties

In order to test the mechanical properties of the reference mixtures, test beams were printed (Figure 5). These beams were then used as such or cut into cubes for the flexural or compression test, respectively (Figure 6). The beams were roughly 40x40x250mm, and the cubes were roughly 40x40x40 mm. Both tests were performed with the specimens in two different layer orientations: horizontal and vertical.

Figure 5. A freshly printed (left) and cured (right) test beam.

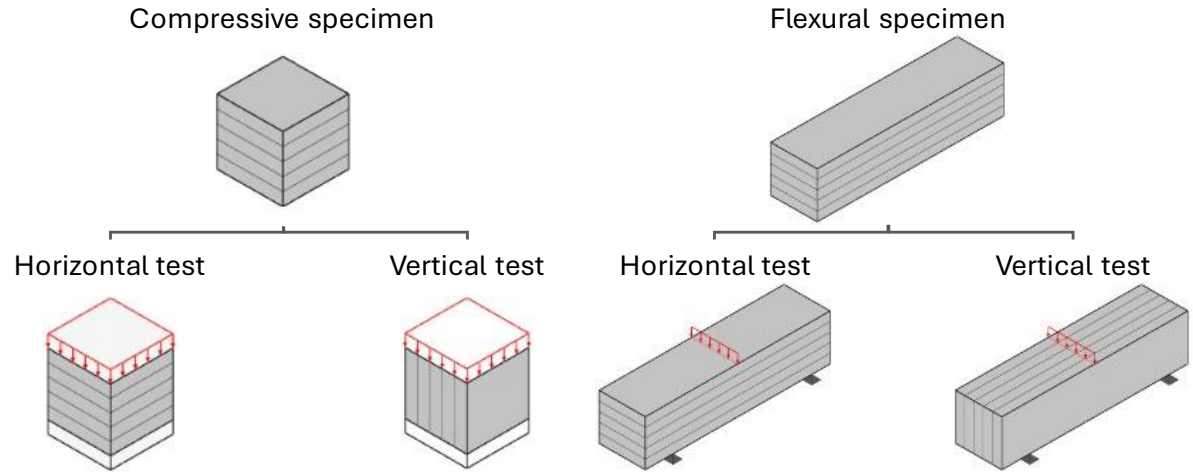

Figure 6. The different specimen orientations used for testing.

The compression test setup was based on the standardised cement mortar test of the NEN-EN 196-1:2016 [50]. The setup consisted of a rigid steel frame (Figure 7) which was placed in the Schenck Trebel test bench, equipped with a 100 kN load cell. The compression test comprised of three cycles, each being repeated three times (sub-cycles). During each cycle, the test was stopped when the desired displacement was reached. These desired displacement for cycles 1, 2 and 3 was 4, 8 and 12 mm, respectively. In order to allow the specimen to recover, the pressure was fully released for one minute between each cycle. Following this, the pressure was increased again until the desired displacement was reached. In this way, the ultimate compressive stress (peak stress reached during the test), compressive strength (peak stress in cycle 1.1) and the compression modulus during cycle 1.1 were established.

Figure 7. The rigid steel frame of the compression test setup.

The flexural tests were three-point bending tests based on the standardised cement mortar test of the NEN-EN 196-1:2016 [50]. The standardised tests have a span of 100 mm, in this research, however, the span was increased to 220 mm to ensure that the specimens are actually subjected to bending and to minimise the effect of the shear stresses. This test determined the ultimate tensile stress, tensile strength and the flexural modulus.

5.1 Wood glue vs bio-glue

Table 5 and Table 6 present the results of the compression tests and the flexural tests, respectively. These data show that, for all compression and flexural tests in both layer orientations, the WG-mixture resulted in higher values for the mechanical properties compared to the BG-mixture, except for the tensile strength, which was the same value for both mixtures. Furthermore, for both mixtures, all flexural tests with a vertical layer orientation yielded higher values for the mechanical properties compared to the horizontal layer orientation, except for the tensile strength, which was the same value.

Table 5. Compressive mechanical properties of the WG and BG mixtures in both layer orientations.

Glue type	Ultimate compressive stress [MPa]		Compressive strength f_c [MPa]		Compression modulus E_c [MPa]	
	Horizontal	Vertical	Horizontal	Vertical	Horizontal	Vertical
Wood glue	16.38	5.87	4.24	3.18	38.36	32.92
Bio-glue	5.13	2.57	1.63	2.52	14.12	20.17

Table 6. Flexural mechanical properties of the WG and BG mixtures in both layer orientations.

Glue type	Ultimate tensile stress [MPa]		Tensile strength f_b [MPa]		Flexural modulus E_b [MPa]	
	Horizontal	Vertical	Horizontal	Vertical	Horizontal	Vertical
Wood glue	3.91	4.70	2.02	2.01	149.29	212.60
Bio-glue	3.86	4.28	2.02	2.01	124.05	166.70

It can be concluded that the WG-mixture is considerably stronger in compression (Table 5) and somewhat stronger in bending (Table 6) in comparison to the BG-mixture. In compression, the WG mixture is stronger when the layers have a horizontal orientation, while the BG mixture is overall stronger when the layers have a vertical orientation. In addition, it can be concluded that the mixtures with a vertical layer orientation are stronger in bending compared to a horizontal layer orientation.
The test results would seem to suggest that the WG-mixture was the optimal choice to proceed with. However, given that the primary objective of this research was to develop a bio-based printable mixture, the bio-based content was considered a crucial factor in the mixture selection. The bio-based content of the WG-mixture is 57%, while the bio-based content of the BG-mixture is 100%. For further experiments, the BG-mixture was therefore selected and will hereafter be referred to as the reference mixture.

5.2 Additives

Three different mixtures were formulated with bio-glue and additives (Table 7) and subsequently tested for their compressive (Table 8) and flexural mechanical properties (Table 9). These data show that all additives improved all compressive mechanical properties of the BG mixture, irrespective of the layer orientation. Furthermore, all additives increased the ultimate tensile stress and the tensile strength of the reference mixture, irrespective of the layer orientation. However, with the vertical layer orientation, all additives decreased the flexural modulus mixture and with the horizontal layer orientation, only the addition of flax increased the flexural modulus.

Table 7. Wood glue and bio-glue mixtures compositions

Additive	Content of component [gram]					
	Cellulose	Lignin	Valida L,3%	Glue	Bentonite	Flax
-	30	300	300	450	-	-
Bentonite	30	300	300	450	37.5	-
Flax	30	300	300	450	-	11.2
Bentonite + flax	30	300	300	450	37.5	11.2

Table 8. Compressive mechanical properties of the BG with additive mixtures in both layer orientations.

Additive	Ultimate compressive stress [MPa]		Compressive strength f_c [MPa]		Compression modulus E_c [MPa]	
	Horizontal	Vertical	Horizontal	Vertical	Horizontal	Vertical
-	5.13	2.57	1.63	2.52	14.12	20.17
Bentonite	11.31	6.76	2.67	5.07	19.83	49.49
Flax	9.17	6.19	2.11	4.77	16.19	44.52
Bentonite + flax	8.53	4.75	2.43	4.38	20.29	44.80

Table 9. Flexural mechanical properties of the BG with additive mixtures in both layer orientations.

Additive	Ultimate tensile stress [MPa]		Tensile strength f_b [MPa]		Flexural modulus E_b [MPa]	
	Horizontal	Vertical	Horizontal	Vertical	Horizontal	Vertical
-	3.86	4.28	2.02	2.01	124.05	166.70
Bentonite	4.37	6.40	3.01	3.03	118.94	117.11
Flax	4.88	6.60	3.02	3.03	128.86	106.53
Bentonite + flax	4.54	4.74	3.02	3.02	129.68	95.30

As the final beam was going to be subjected to bending with the layers in a vertical orientation, the test results of the flexural tests were more important in the selection than the results of the compression tests. The mixture with only flax as an additive had the highest ultimate tensile stress and a medium-high flexural modulus compared to the other additives. These high values for the tensile and flexural mechanical properties led to the conclusion that the BG with flax was the optimal choice for the production of the structural beam.

5.3 Material classification

Figure 8 presents a bubble chart that classifies different families of building materials [51]. The average density of BG with flax beams was 923.73 kg/m^3 (0.92 Mg/m^3). The Young's modulus is equal to the tensile or compression modulus [146]. So, for the BG with flax mixture with a vertical layer orientation, the compression modulus of 44.52 MPa (44.52*10-3 GPa) was used. These values for the density and Young's modulus are indicated with the red lines in Figure 8. This places the BG with flax mixture in the top of the elastomer family. An elastomer is characterized by its elasticity and viscosity, having a low Young's modulus, i.e. leading to large deformations before failure [147]. This was also the case with the BG with flax specimens. However, this is usually considered as an undesired property in a structural material.

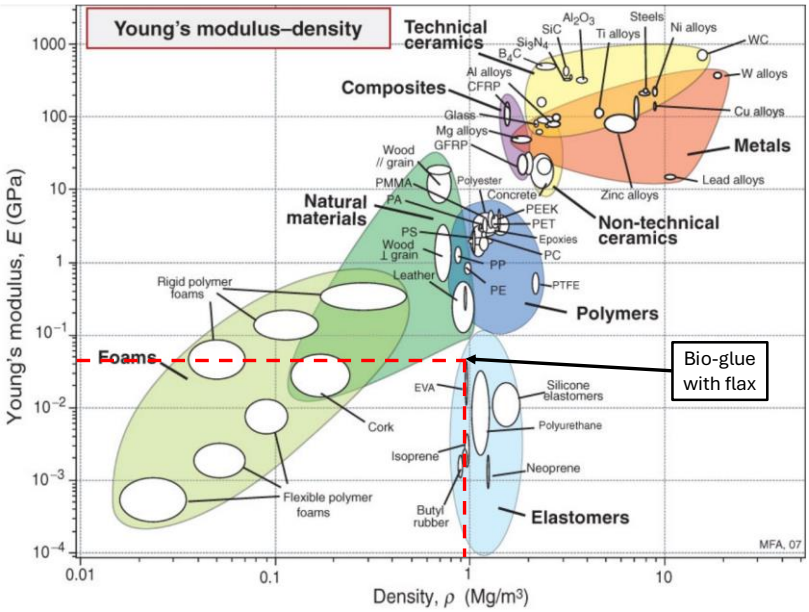

Figure 8. A bubble chart of material families [51].

Table 10 presents the mechanical properties of various wood species, (3D printed) wood composites, 3D printed concrete in comparison with BG with flax mixture. As demonstrated by Figure 8 and Table 10, the current BG with flax mixture is considerably less strong than conventional and comparable building materials, including wood, concrete, steel, wood composites and 3D printed concrete. Its flexural strength is comparable to that some 3D printed wood composites and is higher than that of 3D printed concrete. Due to its low flexural modulus, it is currently unsuitable for use as a building material.

Table 10. Mechanical properties comparison

Material	Flexural strength (tension) [MPa]	Flexural modulus [MPa]	Compressive strength [MPa]	Reference
Bio-glue with flax mixture	6.60	106.53	6.19	[this study]
Beech (American)	86.2 / 7.0 *	9500	50.3 / 7.0 *	[52]
Oak (Overcup)	77.9 / 6.5 *	9800	42.7 / 5.6 *	[52]
Pine (Eastern White)	73.1 / 2.1 *	8500	33.1 / 3.0 *	[52]
Particleboard		2760 – 4140		[52]
MDF		3590		[52]
Plywood		6960 - 8550		[52]
Wood plastic		1530 - 4230	11.7 – 61.2	[52]

15% wood powder 1 UF	19	1930		[33]
17.5% wood powder 1 UF	18	2002		[33]
Methylcellulose-moulded	8.59 - 10.60	670 - 1050		[35], [36]
Methylcellulose-printed	8.48 - 9.55	600 - 640		[35], [36]
Wood glue - moulded	20.67 - 28.89	640 - 900		[35], [36]
89w% wood sawdust MC	2.3 ± 0.4	284.8 ± 46.4		[34]
85.5w% wood sawdust MC	7.4 ± 1.1	733.1 ± 128.0		[34]
3D printed concrete	3 - 3.6		± 30	[53]
3D printed concrete cube			11.3	[54]
3D printed concrete prism			17.51	[54]

**) These data represent "Parallel to grain / perpendicular to grain"*

6 Structural beam

6.1 Lignin shortage

Prior to designing the structural beam, it was determined that different batches of ordered lignin exhibited a significant variation in their properties. This meant that there was a limited amount of usable lignin left. After performing various print tests to determine the printer settings and to find out whether certain connections between print paths were possible. It was concluded that there was just enough lignin left to print a few test beams and one singular structural beam.

6.2 Design

The structural beam was designed using Grasshopper and numerically calculated in GSA. It was designed as a variation of a truss: it consists of a top and bottom chord and diagonals. Firstly, four simplified versions of the beam were analysed and compared (Figure 9). These versions only differed in outer shape. They were all 800 mm long, 240 mm high and were constructed of four layers. Each shape was simply supported by a hinge and a hinged roller. The span between the supports is 780 mm and a load (0.1 kN) is applied in the centre at the top of the element.

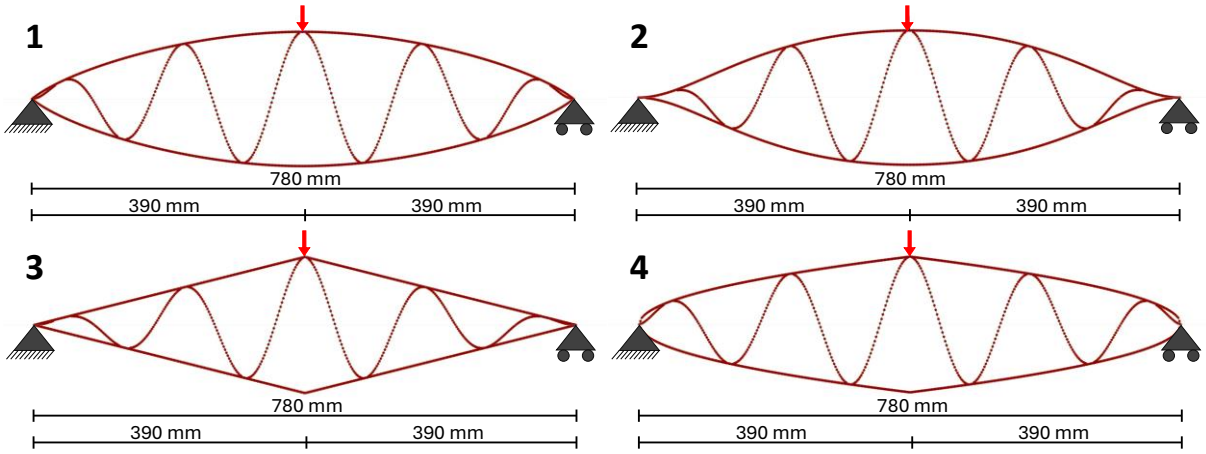

Figure 9. Mechanical schemes of shape 1, 2, 3 and 4.

Using GSA, numerical models were created. The geometric properties of the cross-section are listed in Table 11. The following assumptions were made:

- Each layer has a constant width.
- Each layer has a constant hardened height of 5mm.
- Every layer has the same dimensions.
- Each layer is perfectly printed on top of the layer beneath, the cross-section is thus a perfect square

The material properties used are listed in Table 12. It was assumed that the material was elastic isotropic, and that the flexural modulus and the elastic modulus of the material were equal. Following a sensitivity analysis of the shear modulus and the Poisson's ratio, it was concluded that default values of GSA could be used.

Table 11. Geometric properties of the cross-section.

Name	Width [mm]	Height [mm]	A [cm²]	I_{yy} [cm⁴]
4 layers	20	20	4.00	1.33

Table 12. Material properties.

Elastic modulus (E)	106,5	MPa
Density (ρ)	923,7	kg/m³
Shear modulus (G) ($E/2\,(1+\nu)$)	40,97	MPa
Poisson's ratio (ν)	0,30	-

In GSA, a non-linear analysis was conducted and the vertical displacement, compression and tensile stresses in the element were used for the comparison. After the four different shapes were analysed, shape 1 (Figure 9) was selected as the most optimal outer shape, due to its low displacement and low tensile stresses (for results see Table 13).

Table 13. Outer shape analysis.

Outer shape	Displacement [mm]	Tensile stresses [MPa]	Compressive stresses [MPa]
1	2.509	0.5629	0.7508
2	3.493	0.5925	0.8111
3	4.428	1.1010	0.5785
4	2.769	0.7133	0.6019

The next step was to optimise the infill of the shape. Three different infill variants were analysed and compared (Figure 10). The same geometric and material properties were applied as before. After analysing the three different infills, 7-waves was selected as the most optimal infill, due to its low displacement and stresses (for results see Table 14).

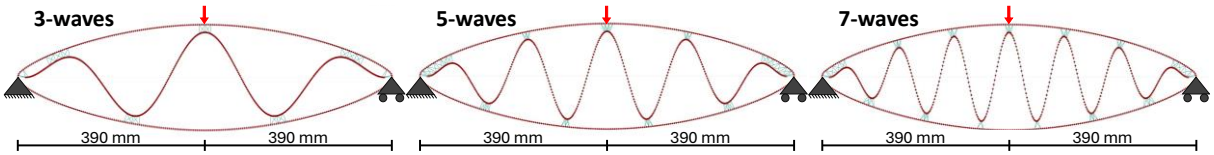

Figure 10. Mechanical schemes of the different infill variants.

Table 14. Infill analysis.

Number of waves	Displacement [mm]	Tensile stresses [MPa]	Compressive stresses [MPa]
3	2.629	0.7194	-0.5772
5	2.131	0.4507	-0.4335
7	2.113	0.3746	-0.4277

The dimensions of the beam described above were determined by the maximum dimensions that could be printed and tested in the SED-lab, rather than by its structural functionality. A width of 20 mm and a height of 240 mm resulted in a relatively slender cross-section. Combined with a length of 800 mm, this created a slender beam, which is disadvantageous its mechanical behaviour. Therefore, Galapagos was used to optimize the dimensions and the adjustable parameters were the length, height and the number of layers (width). For each combination of these parameters, the print length (Figure 11), effective slenderness ratio (Eq. 1, [55].) and the width-to-height ratio (Eq. 2) were determined and kept at or below their ideal value. After the optimisation the beam was 730 mm long, 220 mm high and was constructed of six layers.

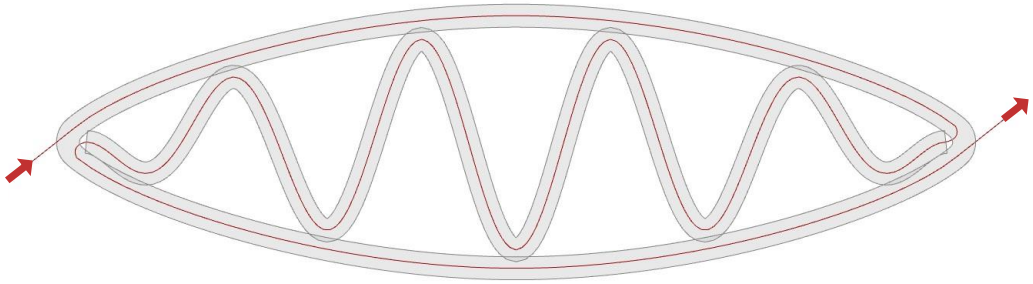

Figure 11. The print path for one layer of the beam. The grey part is the shape, and the red line is the centre line.

$$\lambda_{ef} = L_{ef} * \frac{h}{b^2} < 225 \quad (1)$$

$$width/height\ ratio = 6 < \frac{h}{b} < 8 \quad (2)$$

The print path was designed for a single layer, with an adjustable height to enable printing of all layers. To prevent accumulation of material, the print path was designed without crossing itself. The start and end points were strategically located "outside" the element, ensuring that the replacement of a cartridge and the continuation of printing would not result in interruptions within a layer, thereby preventing formation of weak points in the element. Furthermore, this ensured that the extrusion functioned properly when reaching the main part.

6.3 Final prints

For the sake of clarity, the final prints were made using the BG with flax mixture and Figure 12 shows the names used in this study to identity parts of the structural beam.

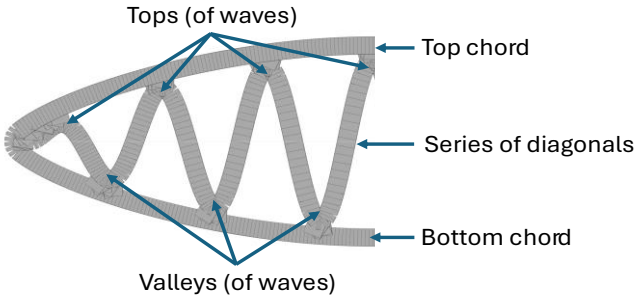

Figure 12. Naming conventions of parts of the beam

First the beam was printed (Figure 13) and with the remaining material five test beams were printed. During the printing process of the structural beam, (significant) misalignments between the layers occurred. Due to the unexpectedly lower height of the fresh layers, the predetermined nozzle standoff distance was incorrect. With the last three layers, this was addressed by manually adjusting the nozzle standoff distance before printing a new layer. However, the previously mentioned misalignment caused various imperfections in the beam, some of which could be fixed manually. Shortly after all layers were printed, a part of the bottom chord next to the second valley fell over and was gently put back by hand (Figure 14).

Figure 13. The freshly printed (1) and cured (2) beam.

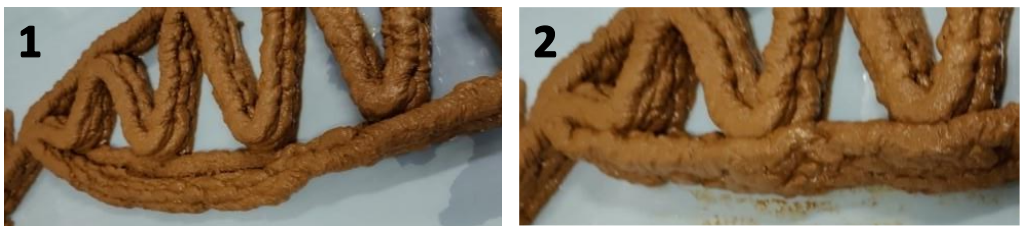

Figure 14. Part of the beam that had fallen (1) but was pushed back up again (2).

The structural beam and the test beams were cured for 40 days in the conditions described above, with additional weights on top of the elements to prevent warping. Furthermore, these weights resulted in compression of the printed material. This led to an increased height shrinkage and a slightly smaller

shrinkage of the length and width. Consequently, the beams had a slightly higher density: 1106.6 kg/m³ instead of 923.7 kg/m³.

6.4 Test results and discussion

To verify the test results of the structural beam, a numerical mesh model with 2D elements was created in GSA (Figure 15). The dimensions of the cured beam were used for this numerical model (cross-sectional dimensions: a width of 27.4 mm and a height of 20.4 mm). This model represented the nodes where the waves and the chords meet more accurately than the line models used with 1D elements (as in previous numerical models) and also the eccentricity in the nodes was fully taken into account.

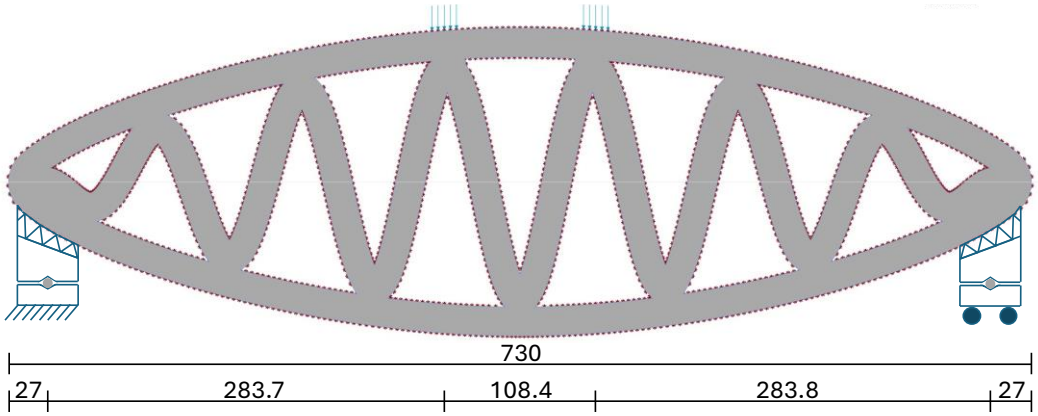

Figure 15. Shape and mechanical scheme of the structural beam, dimensions in mm.

The failure load of the structural beam was determined by trial-and-error analysis. A failure load of 1.63 kN resulted in the maximum tensile stress in the middle of the bottom chord reaching the tensile strength of 3 MPa.

The setup of the structural beam test (Figure 16) was installed in the Instron electromechanical universal testing machine in the SED-lab, which was equipped with a load cell of 5 kN. The test was displacement controlled with a speed of 1 mm/min. The vertical displacement at the middle of the bottom chord was measured with a LVDT sensor and the force applied on the specimen by the machine.

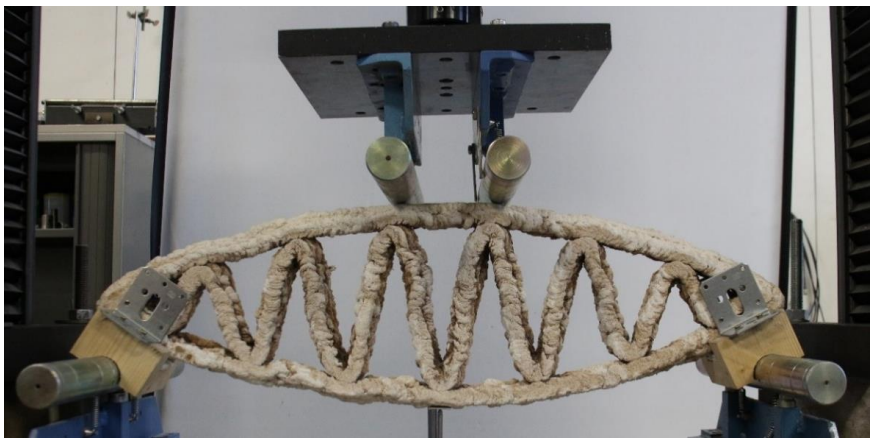

Figure 16. Structural beam test setup up.

Figure 17 presents the force-displacement graph of the structural beam test and Figure 18 shows three photos at different moments of the test. The graph in Figure 17 is relatively linear up to 0.8 kN, after which the slope gradually decreased until the peak force of 1.65 kN was reached. At this moment the accompanying displacement amounted to 24.67 mm.

After this, a wave disconnected from the top chord, which is illustrated in photo 2 in Figure 18. This disconnection led to a significant drop in force (from 1.6 kN to 0.95 kN). The disconnected site of the wave will from now on be referred to as “top 2”. Following this first drop, the test speed was increased to 2 mm/min, which resulted in a minor increase in force. The reason for increasing the test speed, was

that apparently nothing happened after the first drop except for an increasing displacement with the same load.
Shortly after the speed adjustment, a second significant drop in force (from 0.95 kN to 0.4 kN) occurred because the bottom chord fully broke beside the second valley, as illustrated in photo 3. The test was then stopped. This valley where the beam broke at the bottom will henceforth be referred to as "valley 2".

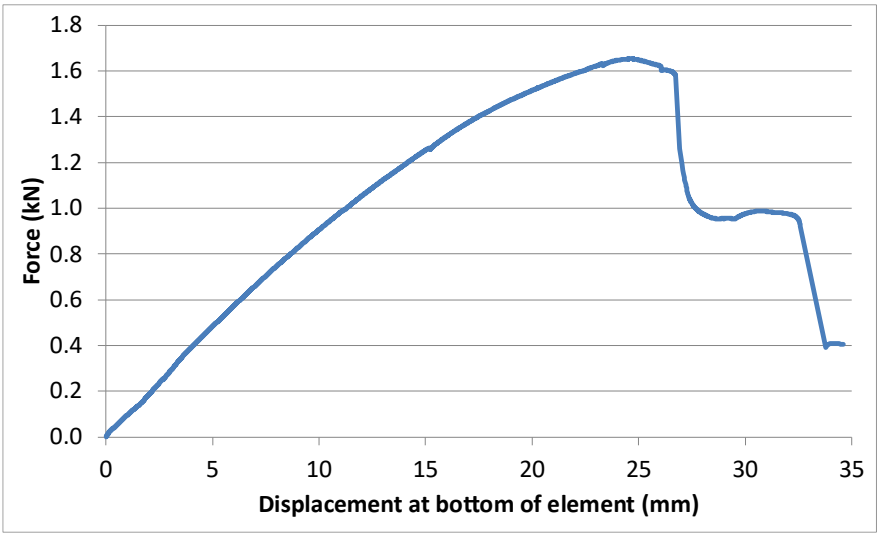

Figure 17. The force-displacement graph of the structural beam test.

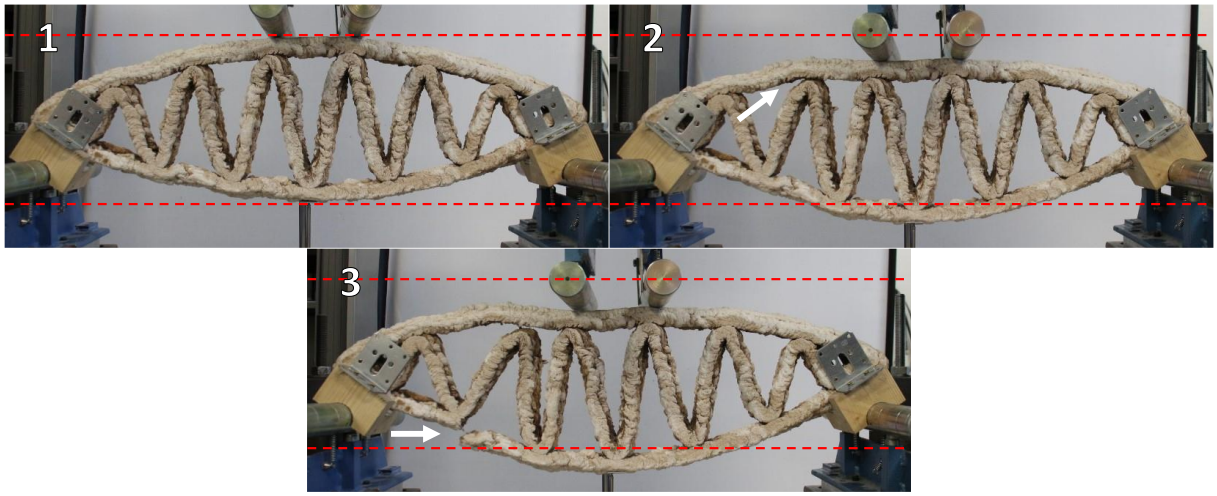

Figure 18. Photos at the start (1), during (2) and at the end (3) of the test, with the red dotted lines indicating the original position of the top and bottom chord.

The expected force from the numerical model in GSA was 1.63 kN, which was slightly exceeded with the structural beam test. As described above, however, the beam behaved not as expected. Furthermore, the measured displacement was significantly higher than expected: 24.67 mm vs 13.10 mm, respectively. This significant difference could be explained by the fact that the model created in GSA is a perfect model, whereas the actual beam had various imperfections. These imperfections could have caused the beam to be less stiff than expected, resulting in a larger displacement than expected. In addition, the faulty connection at top 2 most likely had a considerable impact on the structural behaviour of the beam. Ideally, multiple beams should have been tested to verify the behaviour of the structural beam. However, due to the lignin shortage, this was impossible. In addition, the specific location of the fracture was unexpected. There are several reasons why the beam broke at this particular spot: the material falling over after printing at this spot made it weaker than the rest of the bottom chord and following the disconnection of top 2, the stresses were redistributed, resulting in a stress peak at that particular location.

6.5 Verification

A new GSA model without a connection between top 2 and the top chord, referred to as the "broken wave" model (Figure 19), was used to verify the failure behaviour of the structural beam. This model was analysed with an applied force of 1 kN, which was the maximum force measured prior to the second drop, when the bottom chord broke. The analysis focused on the two parts of the beam, as illustrated below (Figure 20). These parts were analysed separately for both the "broken wave" model and the intact model. The results for the top part are presented in Figure 21, and those for the bottom part in Figure 22. Table 15 presents the maximum results of the compressive stresses in the top chord and the tensile stresses in the bottom chord.

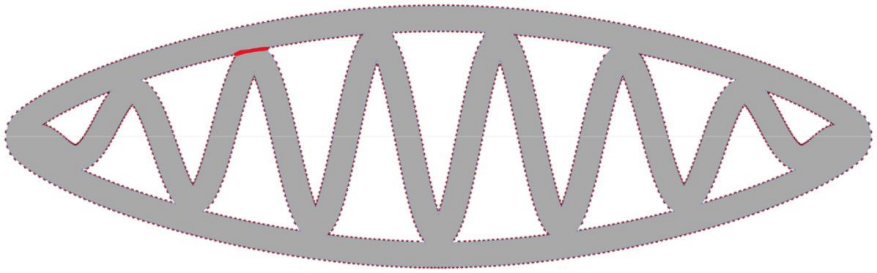

Figure 19. The "broken wave" model in GSA. The red line indicates where the model was split.

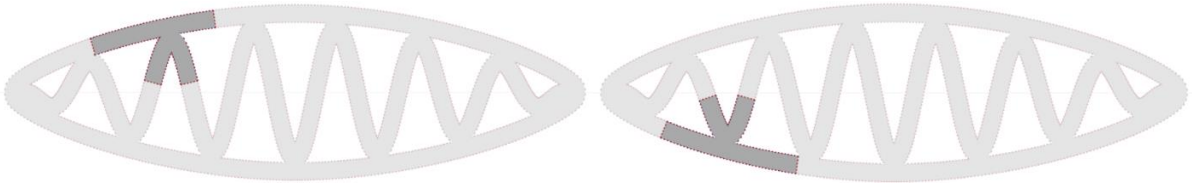

Figure 20. The GSA model with the darker grey part being top 2 in the left model and valley 2 in the right model.

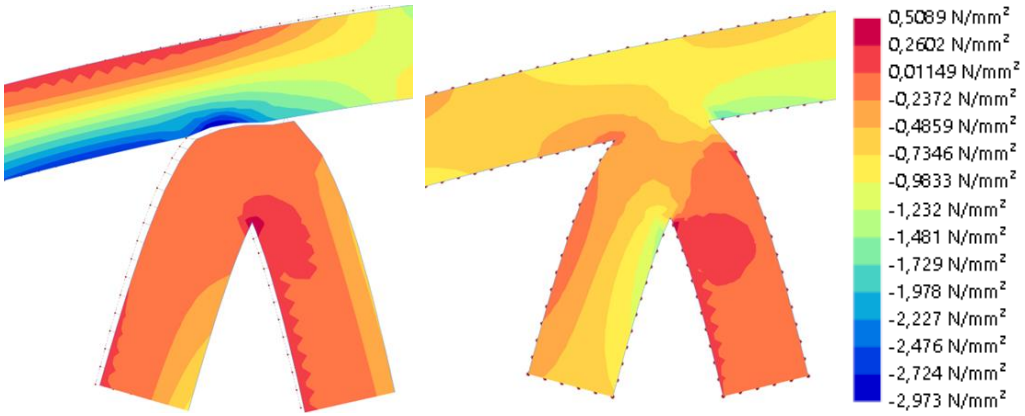

Figure 21. GSA results of the top part of the broken wave model (left) and the intact model (right).

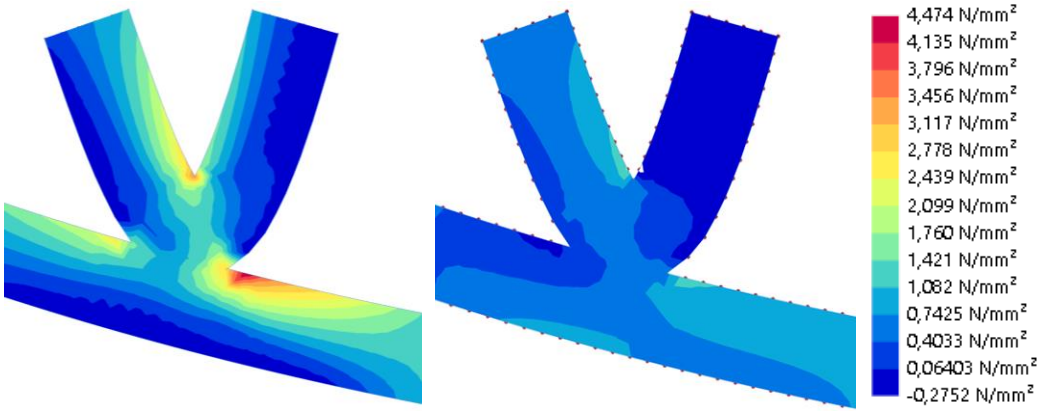

Figure 22. GSA results of the bottom part of the broken wave model (left) and the intact model (right).

Table 15. Results of the GSA analysis of both models.

Model	Compressive stresses in top chord* [MPa]	Tensile stresses in bottom chord** [MPa]
Intact model	-1.785	1.475
"Broken wave" model	-2.973	4.474

**) These stresses occur in the top chord right above wave.*
***) These stresses occur right next to valley.*

Compared to the intact model, the "broken wave" model distributed the stresses significantly different. It resulted in higher compressive stresses in the top chord and higher tensile stresses in the bottom chord. In Figure 22, the high local peak stresses that occur are clearly visible as a red spot on the right of valley 2

During the test it was observed that the top chord buckled upwards, eventually causing the wave to become completely detached from the top chord, resulting in significant higher compression stresses as also shown in the GSA model. The tensile stresses in the bottom chord are three times higher than the stresses recorded in the intact model, causing the beam to break at this particular point.

In addition, the "broken wave" model was analysed with an applied force of 1.65 kN, resulting in a maximum displacement of 21.16 mm. This demonstrates that with the faulty connection, the displacement of the beam is significantly larger . This could indicate that the faulty connection (despite the top not having been completely detached) may have resulted in a larger displacement than expected. The "broken wave" GSA model confirmed the behaviour of the beam during the test, thereby demonstrating the importance of a good connection between different paths. It is clear that, a faulty connection between a wave and the top chord had a substantial negative impact on the stress distribution within this specific element.

7 Conclusion

Digitally designing a structural beam that was optimised for AM, being the objective of this study, was successfully completed. Despite several challenges during the printing process, including layer misalignment and a faulty connection between a wave and the top chord, the structural beam was successfully subjected to a flexural test. After an extra numerical verification, the structural behaviour was validated.

In conclusion, it is possible to produce a digitally designed structural element using AM with a newly developed 100% bio-based material consisting of lignin, cellulose, bio-glue, Valida L,3% and flax fibres. This material demonstrates great potential for the building industry, as its mechanical properties, such as compressive and tensile strength, are comparable to those of other low-strength materials already in use. In terms of sustainability, the material can be produced with locally sourced materials and can be reused in the event of a failed print which is a great advantage

At the moment, the investigated material is clearly not suitable for structural applications or even outdoor settings. The material's current strength and stiffness are not yet structurally safe and further investigation is needed to improve its properties. So, exploring alternatives for certain materials and additives, for example plasticisers or other reinforcing agents, might improve this mixture. In addition, properties such as elasticity, creep, material degradation, fire safety, moisture and UV resistance requires further research. Moreover, the fresh properties and the bond strength between the layers still need to be investigated as these are of great significance in the context of additive manufacturing and the behaviour of freshly printed and cured elements

Acknowledgements

The valuable feedback and support throughout the project by supervisor A.P.H.W. Habraken is highly appreciated. During the early phases of the project, pleasant collaboration with research partner L. Roex is acknowledged. M.T. Ferguson, S.P.G. Moonen and R.J.A Gosselink are acknowledged for their expertise and valuable advice for specific aspects of the project.

This research would not have been possible without the support of the TU/e, Sappi, Wepa and Stora Enso which provided necessary equipment and materials for this project.

References

[1] United Nations, "*What Is Climate Change?,*" Climate Fast Facts. Accessed: Jan. 12, 2023. [Online]. Available: https://www.un.org/en/climatechange/climate-fast-facts

[2] A. Nukusheva, G. Ilyassova, D. Rustembekova, R. Zhamiyeva, and L. Arenova, "*Global warming problem faced by the international community: international legal aspect,*" *Int Environ Agreem*, vol. 21, no. 2, pp. 219–233, 2021, doi: 10.1007/s10784-020-09500-9.

[3] United Nations Environment Programme and Global Alliance for Buildings and Construction, "*Not just another brick in the wall: The solutions exist - Scaling them will build on progress and cut emissions fast. Global Status Report for Buildings and Construction 2024/2025,*" Mar. 2025. Accessed: Apr. 15, 2025. [Online]. Available: https://wedocs.unep.org/20.500.11822/47214

[4] United Nations Framework Convention on Climate Change, "*What is the Paris Agreement?,*" United Nations. Accessed: Jan. 12, 2023. [Online]. Available: https://unfccc.int/process-and-meetings/the-paris-agreement/the-paris-agreement

[5] Ministerie van Infrastructuur en Waterstaat, "*Nederland circulair in 2050,*" 2016. Accessed: Dec. 13, 2022. [Online]. Available: https://www.rijksoverheid.nl/onderwerpen/circulaire-economie/documenten/rapporten/2016/09/14/bijlage-1-nederland-circulair-in-2050

[6] D. Wang, T. Zhang, X. Guo, D. Ling, L. Hu, and G. Jiang, "*The potential of 3D printing in facilitating carbon neutrality,*" *Journal of Environmental Sciences*, vol. 130, pp. 85–91, 2023, doi: https://doi.org/10.1016/j.jes.2022.10.024.

[7] H. Liu, B. Li, and W. Tang, "*Manufacturing oriented topology optimization of 3D structures for carbon emission reduction in casting process,*" *J Clean Prod*, vol. 225, pp. 755–770, 2019, doi: https://doi.org/10.1016/j.jclepro.2019.03.163.

[8] Rural Business-Cooperative Service, "*Biobased Markets Program,*" Department of Agriculture. Accessed: Mar. 18, 2025. [Online]. Available: https://www.federalregister.gov/documents/2024/12/09/2024-28431/biobased-markets-program#page-97465

[9] M. Yadav and M. Agarwal, "*Biobased building materials for sustainable future: An overview,*" *Mater Today Proc*, vol. 43, pp. 2895–2902, 2021, doi: https://doi.org/10.1016/j.matpr.2021.01.165.

[10] N. Keena *et al.*, "*A Life-Cycle Approach to Investigate the Potential of Novel Biobased Construction Materials toward a Circular Built Environment,*" *Energies (Basel)*, vol. 15, no. 19, 2022, doi: 10.3390/en15197239.

[11] B. Dams, D. Maskell, A. Shea, S. Allen, V. Cascione, and P. Walker, "*Upscaling bio-based construction: challenges and opportunities,*" *Building Research & Information*, vol. 51, no. 7, pp. 764–782, 2023, doi: 10.1080/09613218.2023.2204414.

[12] X. Zhai, L. Jin, and J. Jiang, "*A survey of additive manufacturing reviews ,*" *Materials Science in Additive Manufacturing*, vol. 1, no. 4, p. 21, 2022, doi: https://doi.org/10.18063/msam.v1i4.21.

[13] H. Bikas, P. Stavropoulos, and G. Chryssolouris, "*Additive manufacturing methods and modelling approaches: a critical review,*" *The International Journal of Advanced Manufacturing Technology*, vol. 83, no. 1, pp. 389–405, 2016, doi: 10.1007/s00170-015-7576-2.

[14] Applied engineering, "*7 Types of Additive Manufacturing.*" Accessed: Jan. 21, 2025. [Online]. Available: https://www.appliedengineering.com/blog/2021/1/22/7-types-of-additive-manufacturing

[15] S. Tagliaferri, A. Panagiotopoulos, and C. Mattevi, "*Direct ink writing of energy materials,*" *Mater Adv*, vol. 2, no. 2, pp. 540–563, 2021, doi: 10.1039/D0MA00753F.

[16] D. Mondal and T. L. Willett, "*Chapter 23 - Three-dimensional printable nanocomposite biomaterials as bone scaffolds and grafts,*" in *Smart Multifunctional Nano-inks*, R. K. Gupta and T. A. Nguyen, Eds., Elsevier, 2023, pp. 579–594. doi: https://doi.org/10.1016/B978-0-323-91145-0.00002-5.

[17] M. A. S. R. Saadi *et al.*, "*Direct Ink Writing: A 3D Printing Technology for Diverse Materials,*" *Advanced Materials*, vol. 34, no. 28, Mar. 2022, doi: https://doi.org/10.1002/adma.202108855.

[18] G. M. F. Elahee *et al.*, "*On the cogent formulation of an elastomeric silicone ink material for direct ink write (DIW) 3D printing,*" *Polym Eng Sci*, vol. 64, no. 6, pp. 2476–2490, Jun. 2024, doi: https://doi.org/10.1002/pen.26703.

[19] S. Walker *et al.*, "*Predicting interfacial layer adhesion strength in 3D printable silicone,*" *Addit Manuf*, vol. 47, 2021, doi: https://doi.org/10.1016/j.addma.2021.102320.

[20] BCN3D, "*The most popular 3D printing materials in FDM and their properties.*" Accessed: Jan. 31, 2023. [Online]. Available: https://www.bcn3d.com/the-most-popular-3d-printing-materials-in-fdm-and-their-properties/

[21] Mamou-Mani Ltd, "*Conifera.*" Accessed: Jan. 20, 2025. [Online]. Available: https://mamou-mani.com/project/cos/

[22] E. Klarenbeek and M. Dros, "*Weedware©.*" Accessed: Feb. 02, 2023. [Online]. Available: http://weedware.org/

[23] A. Chiusoli, "*The first 3D printed House with earth | Gaia,*" WASP. Accessed: Jan. 20, 2025. [Online]. Available: https://www.3dwasp.com/en/3d-printed-house-gaia/

[24] S. Jordahn, "*3D-printed Gaia house is made from biodegradable materials,*" *Dezeen*, Feb. 27, 2019. Accessed: Feb. 02, 2023. [Online]. Available: https://www.dezeen.com/2019/02/27/gaia-wasp-3d-printed-house-biodegradable-video/

[25] WASP, "*TECLA.*" Accessed: Jan. 20, 2025. [Online]. Available: https://www.3dwasp.com/en/3d-printed-house-tecla/

[26] J. Parkes, "*Tecla house 3D-printed from locally sourced clay,*" *Dezeen*, Apr. 23, 2021. Accessed: Feb. 02, 2023. [Online]. Available: https://www.dezeen.com/2021/04/23/mario-cucinella-architects-wasp-3d-printed-housing/

[27] A. Severi, "*A Wall of 3D Printed Ceramic Bricks,*" *WASP*, Sep. 13, 2024.

[28] O. van Herpt, "*3D Printing Ceramics.*" Accessed: Jan. 20, 2025. [Online]. Available: https://oliviervanherpt.com/3d-printing-ceramics/

[29] A. Finney, "*Arthur Mamou-Mani creates 3D-printed cups for Trame's latest collection,*" *Dezeen*, Mar. 02, 2022. Accessed: Feb. 02, 2023. [Online]. Available: https://www.dezeen.com/2022/03/02/trame-alhambra-rug-ceramic-design-arthur-mamou-mani/

[30] The Exploded View, "*Printed building elements from the water treatment plant,*" The Exploded View Beyond Building. Accessed: Feb. 02, 2023. [Online]. Available: https://theexplodedview.com/materialbb/printed-building-elements-from-the-water-treatment-plant/
[31] M. Fairs, "*Mycelium Chair by Eric Klarenbeek is 3D-printed with living fungus,*" *Dezeen*, Oct. 20, 2013. Accessed: Feb. 02, 2023. [Online]. Available: https://www.dezeen.com/2013/10/20/mycelium-chair-by-eric-klarenbeek-is-3d-printed-with-living-fungus/
[32] J. Hahn, "*Blast Studio 3D prints column from mycelium to make 'architecture that could feed people,'*" *Dezeen*, Jan. 18, 2022. Accessed: Feb. 02, 2023. [Online]. Available: https://www.dezeen.com/2022/01/18/blast-studio-tree-column-mycelium-design/?li_source=LI&li_medium=rhs_block_1
[33] M. Kariz, M. Sernek, and M. K. Kuzman, "*Use of wood powder and adhesive as a mixture for 3D printing,*" *European Journal of Wood and Wood Products*, vol. 74, no. 1, pp. 123–126, Nov. 2016, doi: 10.1007/s00107-015-0987-9.
[34] M. Rosenthal, C. Henneberger, A. Gutkes, and C.-T. Bues, "*Liquid Deposition Modeling: a promising approach for 3D printing of wood,*" *European Journal of Wood and Wood Products*, vol. 76, no. 2, pp. 797–799, 2018, doi: 10.1007/s00107-017-1274-8.
[35] A. A. Coelho, "*Cellulose & Lignin in Additive Manufacturing: Potential and challenges in the fabrication of structural nodes for free-form building envelope structures,*" Delft University of Technology, Delft, 2022.
[36] C. Bierach, "*Wood-based 3d printing: Potential & limitation to 3D print a window frame with pure cellulose & lignin,*" Delft University of Technology, Delft, 2022.
[37] A. Skrebels, "*Sandhelden and Archisource 3D print sand trophies for drawing competition,*" *Dezeen*, Mar. 10, 2022. Accessed: Feb. 02, 2023. [Online]. Available: https://www.dezeen.com/2022/03/10/3d-printed-quartz-sand-trophies-archisource-sandhelden/
[38] Mamou-Mani Ltd, "*The Sandwaves.*" Accessed: Jan. 20, 2025. [Online]. Available: https://mamou-mani.com/project/sandwaves/
[39] L. Crook, "*Chris Precht and Arthur Mamou-Mani use sand to 3D print pavilion in Saudi Arabia,*" *Dezeen*, Jan. 20, 2020. Accessed: Feb. 02, 2023. [Online]. Available: https://www.dezeen.com/2020/01/20/sandwaves-precht-arthur-mamou-mani-pavilion-saudi-arabia/
[40] C. Zarna, M. T. Opedal, A. T. Echtermeyer, and G. Chinga-Carrasco, "*Reinforcement ability of lignocellulosic components in biocomposites and their 3D printed applications – A review,*" *Composites Part C: Open Access*, vol. 6, 2021, doi: https://doi.org/10.1016/j.jcomc.2021.100171.
[41] J. Braun, "*Additives,*" in *Lubricants and Lubrication*, 2017, pp. 117–152. doi: https://doi.org/10.1002/9783527645565.ch6.
[42] G. Zhuang, Q. Li, Z. Zhang, F. Bergaya, and P. Yuan, "*Chapter 2 - Application of bentonite in water-based drilling fluids,*" in *Developments in Clay Science*, vol. 11, G. Zhuang and P. Yuan, Eds., Elsevier, 2024, pp. 21–53. doi: https://doi.org/10.1016/B978-0-443-15598-7.00005-5.
[43] M. Chen *et al.*, "*Rheological parameters, thixotropy and creep of 3D-printed calcium sulfoaluminate cement composites modified by bentonite,*" *Compos B Eng*, vol. 186, Apr. 2020, doi: 10.1016/j.compositesb.2020.107821.
[44] J. P. Dias, F. Brandão, B. Figueiredo, and P. Cruz, "*The potential of natural fiber reinforcement in 3D printed concrete: a review,*" in *DigitalConcrete 2024 - 4th RILEM International Conference on Concrete and Digital Fabrication*, Munich, Germany, Sep. 2024. doi: 10.24355/dbbs.084-202408201106-0.
[45] Y. Lu, J. Xiao, and Y. Li, "*3D printing recycled concrete incorporating plant fibres: A comprehensive review,*" *Constr Build Mater*, vol. 425, 2024, doi: https://doi.org/10.1016/j.conbuildmat.2024.135951.
[46] S. Luhar *et al.*, "*Sustainable and Renewable Bio-Based Natural Fibres and Its Application for 3D Printed Concrete: A Review,*" *Sustainability*, vol. 12, no. 24, 2020, doi: 10.3390/su122410485.
[47] L. Jiang, X. Peng, and D. Walczyk, "*3D printing of biofiber-reinforced composites and their mechanical properties: a review,*" *Rapid Prototyp J*, vol. 26, pp. 1113–1129, Jun. 2020, doi: 10.1108/RPJ-08-2019-0214.
[48] Sappi, "*Valida.*" Accessed: Feb. 10, 2025. [Online]. Available: https://www.sappi.com/nl/valida-home
[49] ABB, "*IRB1200-datasheet,*" 2023.
[50] NEN-EN, "*Methods of testing cement : part 1 : determination of strength,*" in *NEN-EN 196-1:2016*, British Standard, 2016, p. 33. Accessed: Aug. 08, 2024. [Online]. Available: https://www.academia.edu/43087671/Methods_of_testing_cement_Part_1_Determination_of_strength
[51] S. Mackay, "*Materials: Engineering, Science, Processing and Design,*" *Proceedings of the Institution of Civil Engineers - Construction Materials*, vol. 164, no. 4, p. 215, 2011, doi: 10.1680/coma.1000013.
[52] R. J. Ross and F. P. Laboratory. USDA Forest Service., *Wood handbook : wood as an engineering material*. 2010. doi: 10.2737/fpl-gtr-190.
[53] R. J. M. Wolfs, F. P. Bos, and T. A. M. Salet, "*Hardened properties of 3D printed concrete: The influence of process parameters on interlayer adhesion,*" *Cem Concr Res*, vol. 119, pp. 132–140, 2019, doi: https://doi.org/10.1016/j.cemconres.2019.02.017.
[54] Z. Pan, D. Si, J. Tao, and J. Xiao, "*Compressive behavior of 3D printed concrete with different printing paths and concrete ages,*" *Case Studies in Construction Materials*, vol. 18, p. e01949, 2023, doi: https://doi.org/10.1016/j.cscm.2023.e01949.
[55] B. Kuhn, "*Torsion Design of Glulam Beams,*" Dlubal Structural Analysis and Design Software. Accessed: Jun. 03, 2024. [Online]. Available: https://www.dlubal.com/en/support-and-learning/support/knowledge-base/001410